

blood

Prepublished online May 31, 2011;
doi:10.1182/blood-2010-10-312454

Comprehensive analysis of mammalian miRNA* species and their role in myeloid cells

Florian Kuchenbauer, Sarah M. Mah, Michael Heuser, Andrew McPherson, Jens Ruschmann, Arefeh Rouhi, Tobias Berg, Lars Bullinger, Bob Argiropoulos, Ryan D. Morin, David Lai, Daniel T. Starczynowski, Aly Karsan, Connie J. Eaves, Akira Watahiki, Yuzhuo Wang, Samuel A. Aparicio, Arnold Ganser, Jürgen Krauter, Hartmut Döhner, Konstanze Döhner, Marco A. Marra, Fernando D. Camargo, Lars Palmqvist, Christian Buske and Richard Keith Humphries

Information about reproducing this article in parts or in its entirety may be found online at:
http://bloodjournal.hematologylibrary.org/site/misc/rights.xhtml#repub_requests

Information about ordering reprints may be found online at:
<http://bloodjournal.hematologylibrary.org/site/misc/rights.xhtml#reprints>

Information about subscriptions and ASH membership may be found online at:
<http://bloodjournal.hematologylibrary.org/site/subscriptions/index.xhtml>

Advance online articles have been peer reviewed and accepted for publication but have not yet appeared in the paper journal (edited, typeset versions may be posted when available prior to final publication). Advance online articles are citable and establish publication priority; they are indexed by PubMed from initial publication. Citations to Advance online articles must include the digital object identifier (DOIs) and date of initial publication.

Blood (print ISSN 0006-4971, online ISSN 1528-0020), is published weekly by the American Society of Hematology, 2021 L St, NW, Suite 900, Washington DC 20036.

Copyright 2011 by The American Society of Hematology; all rights reserved.



Regular Article - MYELOID NEOPLASIA

Comprehensive analysis of mammalian miRNA* species and their role in myeloid cells

Florian Kuchenbauer^{1,2,3}, Sarah M. Mah³, Michael Heuser⁵, Andrew McPherson⁴, Jens Ruschmann³, Arefeh Rouhi², Tobias Berg³, Lars Bullinger¹, Bob Argiropoulos³, Ryan D. Morin⁴, David Lai³, Daniel T. Starczynowski³, Aly Karsan³, Connie J. Eaves³, Akira Watahiki⁶, Yuzhuo Wang⁶, Samuel A. Aparicio⁷, Arnold Ganzer⁵, Jürgen Krauter⁵, Hartmut Döhner¹, Konstanze Döhner¹, Marco A. Marra⁴, Fernando D. Camargo⁸, Lars Palmqvist⁹, Christian Buske² and Richard Keith Humphries³

¹Department of Internal Medicine III, University Hospital of Ulm, Ulm, Germany; ²Institute of Experimental Cancer Research, Comprehensive Cancer Centre, University Hospital of Ulm, 89081 Ulm, Germany; ³Terry Fox Laboratory, BC Cancer Agency, Vancouver, BC, Canada, V5Z 1L3; ⁴Canada's Michael Smith Genome Sciences Centre, Vancouver, BC, Canada, V5Z 1L3; ⁵Medizinische Hochschule Hannover, 30625 Hannover, Germany. ⁶Department of Cancer Endocrinology, BC Cancer Agency, Vancouver, BC, Canada, V5Z 1L3; ⁷Department of Molecular Oncology, BC Cancer Agency, Vancouver, BC, V5Z 1L3; ⁸Whitehead Institute for Biomedical Research, Cambridge, Massachusetts 02142, USA; ⁹Institute of Biomedicine, Sahlgrenska University Hospital, University of Gothenburg, Sweden

Corresponding author:
R. Keith Humphries MD, PhD
675 West 10th Ave
Vancouver, V5Z 1L3
Canada
Phone: 604-6758140
Fax: 604-877-0712
Email: khumphri@bccrc.ca

Running title: miRNA*s in myeloid cells

Key words: microRNA, microRNA*, myeloid differentiation

Abstract

Processing of the pre-miRNA through Dicer1 generates a miRNA duplex, consisting of a miRNA and miRNA* strand. Despite the general view that miRNA*s have no functional role, we further investigated miRNA* species in 10 deep sequencing libraries from mouse and human tissue. Comparing miRNA/miRNA* ratios across the miRNA sequence libraries revealed that 50% of the investigated miRNA duplexes exhibit a highly dominant strand. Conversely, 10% of miRNA duplexes show a comparable expression of both strands, while the remaining 40% exhibit variable ratios across the examined libraries as exemplified by miR-223/miR-223* in murine and human cell lines. Functional analyses revealed a regulatory role for miR-223* in myeloid progenitor cells, implying an active role for both arms of the miR-223 duplex. This was further underscored by the demonstration that miR-223 and miR-223* target the IGF1R/PIK3 axis and that high miR-223* levels associate with increased overall survival in acute myeloid leukemia (AML) patients. Thus, we found a supporting role for miR-223* in differentiating myeloid cells in normal as well as the leukemic cell state. The fact that the miR-223 duplex acts through both arms extends the complexity of miRNA-directed gene regulation of this myeloid key miRNA.

Introduction

The canonical miRNA biogenesis pathway involves the stepwise processing of miRNA precursor transcripts containing hairpin structures in the nucleus as well as in the cytoplasm¹. After processing through Drosha in the nucleus, miRNA containing hairpins are exported into the cytoplasm and cleaved by Dicer, resulting in a ~21-25nt miRNA duplex². Although both strands of miRNA duplexes are necessarily produced in equal amounts by enzymatic processing, their accumulation is mainly asymmetric at steady state. Depending on its frequency, the most abundant strand of a processed pre-miRNA is referred as miRNA, whereas the less abundant strand is known as “passenger strand” or miRNA* (read miRNA star)³⁻⁵, initially annotated by the first miRNA sequencing approaches⁶⁻⁹. Although the mechanism of miRNA strand selection and RNA induced silencing complex (RISC) loading are still unclear, studies on siRNA duplexes indicated that the relative thermodynamic stability of the two ends of the duplex determines which strand is to be selected^{3,4}. The strand with relatively unstable base pairs at the 5' end typically evades degradation^{3,4}. Thermodynamic stability profiling studies on miRNA precursors suggested that the same rule might apply to most, although not all, miRNAs³.

Recent profiling approaches from our group¹⁰⁻¹² and others^{13,14} aimed at detecting and quantifying small RNA species demonstrated not only the presence of miRNA*s strands across species, but also their high abundance for certain miRNA duplexes. The incorporation of miRNA*s into the RISC was shown recently in *Drosophila melanogaster*^{15,16}. Moreover, luciferase reporter assays have provided evidence for the functionality of both miRNA strands¹⁷.

Furthermore, SNPs identified within the pre-miR-146 hairpin and seed region of miR-146* are purported to change its target specificity^{18,19}.

Considering that every miRNA duplex consists of a miRNA and miRNA*, it is interesting to note that only 8.1% of miRNA*s (80 miRNA* out of 940 miRNAs, miRBase 15.0) in the human genome have been annotated. This is likely due in part to the low expression levels of certain miRNA*s, and also the fact that miRNA* sequences have only recently been added to miRNA microarrays and Taqman probe libraries. The advent of next generation sequencing has dramatically increased the ability to sensitively, comprehensively and quantitatively assess the pattern of miRNA and miRNA* species. To this end we analyzed 10 deep sequencing libraries derived from different model organisms, solid tumors and in particular leukemias to determine the expression levels of known and non-annotated miRNA*s compared to their cognate miRNA strands. This comprehensive approach allowed us to identify tissue and species-independent patterns of miRNA/miRNA* expression, which suggested a novel classification for miRNA duplexes. Differential ratios of miRNA to miRNA* were also revealed as illustrated by the dramatic differential expression of miR-223 and miR-223* in normal myeloid as well as pathophysiological myeloid conditions.

Materials and Methods

Small RNA Library Preparation

Previously published libraries for undifferentiated and differentiated H9 hESC cells as well as murine ND13 (mouse leukemia 1) and ND13+Meis1 (mouse leukemia 2) cell lines were re-annotated according to miRBase 13.0^{10,11}. Furthermore, 3 human leukemia cell lines (Leukemia 1-3), 2 libraries derived from human prostate cancer tissue (prostate 1 and prostate 2) and one library derived from a human colon cancer cell line (colon) were generated as previously published¹⁰. Short RNA sequences from each library were aligned to the human genome (NCBI36) for human derived libraries and to the mouse genome (NCBIM37) for murine derived libraries. Small RNA sequences were filtered by considering only those sequences with alignments that overlapped with mature miRNA or miRNA* annotations as found in miRBase 13.0. Sequence counts for each miRNA and miRNA* were considered to be the counts of the total number of sequences in the library as previously described^{10,11}. In some cases, we found evidence of the expression of a miRNA* sequence with no annotation in miRBase. Expression for unannotated miRNA* sequences was calculated as the count for the most abundant sequence that was approximately reverse complementary with the miRNA sequence. To qualify as a potential miRNA*, a sequence required an alignment to the region of the stemloop with complimentary to the mature miRNA sequence, plus or minus 5 nucleotides at each end. Ratios between miRNA and miRNA* were calculate as (miRNA counts+1):(miRNA* counts +1) providing a well defined measurement for the possibility of miRNA* sequences with no stable expression. See **Table S5** for total number of reads

and alignment efficacy.

Retroviral vectors and cDNA

All murine miR-223 constructs (miR-223, miR-223mut and miR-223*mut) were ordered from Integrated DNA Technologies (IDT, www.idtdna.com) and cloned into a murine stem cell virus (MSCV) construct as previously described²⁰. In all constructs the published IRES cassette was replaced with a PGK promoter sequence, driving enhanced green fluorescent protein (eGFP) expression. All construct sequences are listed in **Supplementary Experimental Procedures S1**.

Retroviral infection and Clonogenic progenitor assay

Whole mouse bone marrow from miR-223 deficient mice as well as wild-type mice²¹ was extracted, lysed with NH₄Cl and stimulated for 48 hours in DMEM supplemented with 15% FBS, 10 ng/ml hIL-6, 6 ng/ml mIL-3 and 100 ng/ml mSCF (StemCell Technologies Inc.; Vancouver, BC, Canada). The cells were transduced by co-cultivation with irradiated (4,000 cGy) viral producers in the presence of 5µg/ml protamine sulfate (Sigma, Oakville, Canada; Cat. No. P4020) for 48 hours. GFP positive cells were FACS sorted into 15ml falcon tubes containing 3ml methylcellulose (Methocult M3434; StemCell Technologies) supplemented with cytokines as previously described²². The gene transfer ranged from 2%-5%. Colonies were counted and evaluated 7 days after plating by standard criteria.

Real-time PCR

RNA was extracted using Trizol (Invitrogen, Carlsbad, CA) as previously described¹¹. Reverse transcription of each miRNA or sno-202 was performed using the Taqman miRNA Reverse Transcription Kit (Applied Biosystems, Foster City, CA) according to the manufacturers instructions. Each patient RNA sample was measured using Nanodrop (Thermo Scientific) and equilibrated to a concentration of 5ng/ml. 20ng RNA were used for miR-223* specific reverse transcription. 5ng RNA from a healthy bone marrow donor was used as standard for calculating DDCT values and fold changes. MiR-92 was used as a housekeeping gene for all human samples²³ and sno-202 for murine samples. Quantitative reverse transcription-polymerase chain reaction (RT-PCR) was performed using miR-223 (ABI#4395406), miR-223* (ABI#4395209), miR-92 (ABI#4373013) and sno-202 (ABI#4380914) ABI Taqman probes on an Applied Biosystems 7900HT Fast Real-Time PCR system in triplicates. Reverse transcription of total mRNA was performed using random primers and the Superscript III (Invitrogen, Carlsbad, CA) as previously described²⁴. Real-time PCR on coding genes was performed using SYBR green (Invitrogen, Carlsbad, CA) as previously described²⁴. All primers are listed in **Table S6**.

Luciferase assays

Predicted (TargetScan custom v5.0, hsa-miR-223* seed: GUGUAUU) miR-223* binding regions of IGF1R (chr15:99501790-99502039) were cloned into pMIR-REPORT (Ambion, Austin, Tx) and transfected with hsa-miR-223* (Thermo Scientific Dharmacon, Lafayette, USA), a scrambled control

(Ambion, Austin, Tx) or a negative control miRNA (Ambion, Austin, Tx) into 293T cells. For the 3'UTR-luciferase assays, 20 ng of pMirReport-3'UTR, 10pmol of miRNAs and 0.17 ng of thymidine kinase-renilla were cotransfected into 4×10^5 293T cells (48-well format) using the Lipofectamine 2000 transfection reagent (Invitrogen, Burlington, CA). The assays were read in the Lumat LB 9507 tube luminometer (EG&G BERTHOLD, Germany) and the Luciferase/Renilla ratio calculated. Student's t-test was used for statistical analysis and $p < 0.05$ considered as significant.

Retroviral infection of murine bone marrow cells

Total bone marrow (BM) from miR-223 knockout (mir-223^{-/-}) and wildtype (miR-223^{+/+}) mice ²¹ was extracted, prestimulated for 2 days as previously described ²⁴. Then, the BM cells were simultaneously cotransduced with MSCV-*Hoxa9*-pgk-*neomycin* and a MSCV-*Meis1*-IRES-*YFP* by co-cultivation with irradiated (4,000 cGy) viral producers as previously described ²⁴. *HoxA9*-*Meis1* transduced cells were sorted for YFP expression and continuously selected with neomycin (1.4 mg/ml).

Microarrays

RNA from the above described bone marrow cell lines was extracted using Trizol (Invitrogen, Carlsbad, CA) as previously described ¹¹. The extracted RNA further cleaned using the miRNA easy kit (Quiagen, Düsseldorf, Germany) according to the manufacturer's instructions. The Affymetrix Mouse Gene 1.0 ST Array was used to generate gene expression data on 2 biological replicates. Gene expression array data (CEL-files) was analysed

using the software GeneSpring® GX 11.5.1 (Agilent Technologies). The exon RMA 16 algorithm and quantile normalization was used and the median of all the samples in each experimental setting was used for baseline transformation. Genes were then filtered according to expression of the 20.0 - 100.0th percentile of the raw data and tested for significance (one-way Welch-ANOVA, corrected p-value cut-off =0.05). The MIAME (minimal information about a microarray experiment) guidelines have been followed for data presentation. All microarray data are available at the Gene Expression Omnibus (GEO) under accession number GSE29453.

Statistical analysis

Statistical analysis for overall survival and correlation of clinical parameters was performed as previously described ²⁵. The definition of overall survival (OS) followed recommended criteria ²⁶. In brief, AML samples were dichotomized at the median, the 25th and the 75th percentile of the miR-223* real time expression value. The Kaplan-Meier method and log-rank test were used to estimate the distribution of overall survival (OS) and to compare differences between survival curves. Pairwise comparisons were performed by Student t test for continuous variables and by chi-squared test for categorical variables. The 2-sided level of significance was set at P values less than .05. The statistical analyses were performed with the statistical software package SPSS 15.0 (SPSS Science, Chicago, IL).

Further details about patient collectives and performed methods can be found under **Experimental Procedures S1**. For all patients, written informed

consent was obtained prior to therapy according to the Declaration of Helsinki, and the study was approved by the institutional review board of Hannover Medical School.

Results

The abundance of miRNA*s is tissue dependent

We investigated the expression and relationship of miRNAs and their corresponding miRNA*s in 10 Illumina sequencing libraries derived from murine and human cell lines and tissues. In detail, we analyzed the miRNA expression profile of two murine hematopoietic libraries, a mouse pre-leukemic myeloid cell line (mouse leukemia 1) [NUP98-HOXD13 (ND13)] and its leukemic counterpart (mouse leukemia 2) (ND13+Meis1), derived from transformed mouse bone marrow cells with a *NUP98-HOXD13* fusion gene and the HOX co-factor Meis1¹¹. In addition, we analyzed undifferentiated (ES undiff) and differentiated (ES diff) embryonic stem cell libraries¹⁰, three common human leukemia cell lines (human leukemia 1-3)²⁷, two libraries derived from human prostate cancer tissue (prostate 1 and prostate 2) and one library derived from a human colon cancer cell line (colon). The miRNA expression profile of each library was analyzed. The expression level of a mature miRNA or miRNA* was calculated by the total number of sequences in the library that found a best hit alignment to that miRNA or miRNA*.

All libraries were analyzed according to the sum of all sequences^{10,11} and only miRNA/miRNA* pairs originating from the same stemloop structure were considered for analysis if either the miRNA or miRNA* showed an expression level greater than or equal to 100. The varying sequencing depth of the libraries ranged from 666,362 to 4,661,901 miRNA reads and 5,273 to 130,652 miRNA* reads (**Table 1**).

Across all libraries, the percentage of all detected miRNA* species compared to all detected miRNAs varied from 0.3% to 12.3% (**Table 1**), as pictured for ES cells in **Figure S1A**, suggesting tissue-dependent expression levels of miRNA*s. The highest percentage of miRNA* species was detected in the ES undiff library (12.3%), whereas the lowest percentage was detected in the prostate 2 library (0.3%) (**Table 1**). Classification of the miRNA/miRNA* ratio into groups (**Table 2**), showed that ~50% of all miRNA duplexes (range: 40.7 to 61.2%) revealed high ratios (>100) consistent with strong preferential processing of one dominant miRNA strand. A significant proportion, ~24%, (range: 18.1 to 30.9%), had intermediate ratios (between 100 and 10) and strikingly, ~13% (range: 8.6-17.7%) showed low ratios (between 10 and 1). In addition, ~13% (range: 7.1-19.1%) showed inverted ratios (<1) (**Table 2**). These findings oppose the general assumption that only one strand is highly dominant for any given miRNA duplex. Moreover, high strand abundance also was detected for some members in the low ratio groups, indicating a weak correlation between strand abundance and miRNA duplex ratio (**Figure S1B**). In addition, the observation that >10% of all miRNA duplexes displayed an inverse ratio is indicative that incorrect annotations are documented in miRBase (**Table S1** for all ratios across all libraries, **Table S2** for all ratios > 100 sequence counts, **Table S3** for all sequences and sequence counts for each individual library).

miRNA*s can be classified according to their abundance in relation to the corresponding miRNA

Based on the finding that the distribution of miRNA/miRNA* ratios grouped similarly in all libraries, we asked whether the ratios for individual miRNA duplexes remained constant or changed across all investigated tissues. Indeed, most miRNA duplexes preserved their miRNA/miRNA* distribution across the different libraries (**Figure 1A, Table S1, Table S2, Table S3**). Based on this, it is possible to classify miRNA duplexes into α -duplexes, having a dominant strand with a ratio >10 such as the let-7 family, β -duplexes exhibiting relatively balanced ratios ≥ 0.1 and ≤ 10 , spanning approximately one order of magnitude, such as miR-17 and miR-425 (**Figure 1A, Table 3**). However, 7 miRNAs were characterized by a dynamic arm expression with ratios ranging between >10 and <1 and therefore interchanging dominant miRNA arms between the different tissues (**Figure 1B, Table 4**). This phenomenon was independent of conservation as demonstrated by oscillating miRNA arm expression between the investigated libraries for both, poorly conserved miRNA duplexes such as miR-1307 as well as broadly conserved duplexes, such as miR-223 (**Figure S1D**).

MiR-223 and miR-223* accumulation is a dynamic process

The finding that certain miRNAs displayed tissue-dependent miRNA arm selection, prompted interest in the possible biological function of selective accumulation of miRNA* strands. Of the reported miRNAs in **Figure 1B**, miR-223, a known regulator of myeloid differentiation^{21,28,29}, is the best functionally characterized miRNA in hematopoietic tissue. Lentiviral overexpression of hsa-miR-223 in NB4 cells, a promyelocytic leukemia cell line, led to further differentiation of these cells^{29,30}, underscoring its role in myeloid differentiation. Interestingly, miR-223 and miR-223* were differentially

expressed in the investigated tissues, especially in the ND13 (mouse leukemia 1) and ND13+Meis1 (mouse leukemia 2) leukemia progression model (**Figure 1B**). Specifically, miR-223* was enriched by ~30 fold in the ND13 myeloid progenitor line compared to its leukemic counterpart ND13+Meis1 (3366 vs. 115 counts), and miR-223* sequence counts also exceeded miR-223 (¹¹ and **Figures 1B, S1C**). This dynamic pattern could be observed across all bone marrow derived libraries, regardless of human or mouse origin (**Figure S1C**), implying that miR-223* contribute to the function of miR-223. In contrast, other bone marrow specific miRNAs showed a more constant expression pattern (**Figure S1C**). Variable miR-223* levels and the fact that miR-223 as well as miR-223* remained broadly conserved in vertebrates (**Figure S1D**) pointed towards a miRNA duplex with two functional arms. Considering that ectopic expression of miR-223 involves overexpression of pri-miR-223 ^{28,29}, which includes expression of both miRNA duplex arm, it remains unknown whether miR-223* contributes to the observed phenotype.

miR-223* decreases the colony-forming capacity of miR-223 deficient bone marrow cells

In order to test possible functions of both miR-223 and miR-223* in hematopoietic cells, we exploited a murine miR-223 knockout (miR-223KO) model ²¹. Previous analysis of miR-223 deficient bm revealed an enhanced number of myeloid progenitors as well as impaired differentiation of granulocytes ²¹. In order to assess the influence of miR-223* in myeloid progenitor cells, we used a retroviral construct engineered to render the seed

region of the miR-223 arm inactive (miR-223mut) (**Figure 1C**). Wildtype and miR-223KO bm transduced with miR-223 or miR-223mut were plated and their colony-forming capacity was assessed (**Figure 1D**). CFC progenitor numbers were elevated in the miR-223 knockout background ($p=0.0171$). Overexpression of miR-223* using the miR-223mut construct significantly reduced the CFC output ($p=0.008$), highlighting the regulatory potential of miR-223* (**Figure 1D**). These findings suggest that miR-223 and miR-223* might have separate functions that complement each other. Specific knockdown of the miR-223 strand has been shown to impair differentiation in granulocytes²¹, whereas our results imply a regulatory role of miR-223* in proliferation or self-renewal of myeloid progenitor cells. These results demonstrate a role for miR-223* in primary hematopoietic cells.

miR-223* and miR-223 target the IGF1R pathway

To investigate further possible functions of miR-223*, we used bioinformatics to predict conserved targets with Targetscan custom (v5.0, www.targetscan.org) using the 7nt seed sequence (GUGUAUU) of hsa-miR-223* as well as the predicted targets of hsa-miR-223 (**Figure S2A, Table S4**). Interestingly, both arms are predicted to regulate IGF1R signaling, a pathway implicated in normal and malignant hematopoiesis. Therefore, to further identify differentially expressed targets between miR-223 wildtype (WT) and miR-223 knockout (KO) cells, we performed a mRNA microarray expression analysis on immortalized miR-223 bone marrow cells. In our analysis, we found a set of 1264 differentially expressed genes (743 genes upregulated, 521 downregulated) between miR-223KO and miR-223WT cells ($n=2$, $p<0.05$)

(Table S4). Comparing the differentially expressed genes with predicted targets for mmu-miR-223 and mmu-miR-223* (www.targetscan.org), 2 genes **(Figure 2A)**, *Fam120c* (1.078 fold, $p=0.006$), a gene linked to autism and *Igf1r* (1.37 fold, $p=0.04$), a gene linked to the IGF1R/PIK3 axis, a gene involved in hematopoietic malignancies³¹⁻³⁴, overlapped between both prediction lists. These findings suggest a shared regulation of the IGF1R/PIK3 axis by miR-223 and miR-223*. In further support of this, the effect of miR-223 depletion was significantly reversed for *Igf1r* by retroviral overexpression of miR-223* (miR-223mut, 1.13 fold, $p=0.043$) and selectively with miR-223 (miR-223*mut, 1.11 fold, $p=0.043$) **(Table S4)**. To confirm and extend these findings, we used quantitative real-time PCR analysis³⁵ to quantify 12 predicted miR-223* targets (*Cux1*, *Igf1r*, *Neo1*, *Pi3kcd*, *Dlc1*, *Lyn*, *Ube2*, *Fgf7*, *Sema3a*, *Slc2a*, *Pten* and *Lpp*) implicated in normal as well as leukemic development. After filtering, using a threshold of a 1.5 fold increase in miR-223KO cells, *Cux1*, *Dlc1*, *Pik3cd* and *Igf1r* remained as possible targets of miR-223* **(Figure 2B)**. In further support of this, the effect of miR-223 depletion was significantly reversed for all 4 targets by retroviral overexpression of miR-223* (using the miR-223mut construct) **(Figures 2B and S2B)**. As predicted, with a similar approach with an inactivated miR-223* arm (miR-223*mut) to thus selectively overexpress miR-223, *Igf1r* levels exhibited a significant decrease, indicating a regulatory role for both miR-223 and miR-223* ($p=0.029$ and $p=0.04$, respectively) in the expression of *Igf1r*. However, our in vitro data also indicates that miR-223 might have a higher binding affinity than miR-223* as lower miR-223 levels show a similar *Igf1r* knockdown **(Figure 2B, Figure S2B)**. The regulatory potential of miR-223* on

IGF1R was also confirmed through an in vitro luciferase assay ($p=0.018$) (**Figure 2C**). Combined, these results raise the intriguing possibility that miR-223* plays a cooperative role with miR-223 by targeting the same transcript within the IGF1R/PIK3 axis, a key pathway for developmental and malignant processes^{36,37}.

miR-223* levels correlate with prognostic markers in AML patients

Considering that in vitro inhibition of IGF1R signaling also affects leukemic blasts³³ and leads to the inhibition of colony formation of acute myeloid leukemia (AML) blasts³⁸, we examined miR-223 and miR-223* expression levels in normal and malignant cells and if they correlate with clinical parameters of AML patients. Therefore, we quantified miR-223* and miR-223 expression by real-time PCR in 92 AML patients under the age of 60 years with normal cytogenetics (CN-AML) (**Table 5**) and 10 healthy donors. In line with our sequencing libraries, miR-223* levels in AML samples as well as in normal hematopoietic samples only showed a moderate positive correlation with the expression of miR-223 ($R^2=0.2351$, $R^2=0.0729$, respectively) (**Figure S2C**), underscoring its variable expression. We found miR-223* to be significantly higher expressed in healthy donors ($p=0.016$) compared to AML patient samples (**Figure 2D**). Interestingly, with a dichotomization to the 75th percentile, high miR-223* expression levels associated significantly with superior overall survival ($p=0.016$) (**Figure 2E**). In contrast, miR-223 did not associate with any survival parameters, regardless of dichotomization. Both miRNAs did not correlate with any other clinical parameter (**Table 5**),

indicating, that the correlation between high miR-223* levels and increased survival is not confounded by other clinical variables.

Discussion

Here we have exploited the recent availability of next generation deep sequencing data from 10 different libraries to enable a comprehensive, quantitative analysis of miRNAs and the corresponding miRNA*s. Our results provide evidence that relative miRNA and miRNA* expression is conserved between various tissues and cell lines, allowing for a novel classification and prediction of possible functional miRNA and miRNA* strands, derived from one duplex. Intriguingly, for select miRNAs, such as miR-223/miR-223*, the miRNA/miRNA* ratios exhibited considerable variability across libraries. Further investigation of miR-223* in vitro suggest a functional role in concert with miR-223 in myeloid cells; in addition, high miR-223* levels were associated with a higher overall survival in CN-AML patients.

Across all examined libraries, the proportion of miRNA*s to miRNAs ranged between 0.3% and 12.3%, indicating that the overall miRNA* expression is tissue and species-dependent. Comparison of all the sequencing libraries derived from different tissues revealed conserved patterns between miRNA and the corresponding miRNA* arms. Besides instances with highly dominant miRNA arms, such as the highly abundant let-7 family, we also found instances with balanced expression of the miRNA and miRNA* species such as miR-30e, confirming previous findings by Ro et al.¹⁷. We termed miRNA duplexes that give rise to a dominant strand α -duplexes and duplexes that give rise to a more balanced strand expression, β -duplexes. This novel classification carries with it the important prediction of whether one or in case of a β -duplex, both miRNA strands are functional active. In addition, we found several miRNAs where the annotated miRNA* arm is strongly dominant over

the miRNA arm, indicating improper annotation in miRBase, such as miR-129* and miR-517*. Furthermore, we are able to unambiguously annotate the miRNA* strand of miRNAs such as miR-423 and miR-371. Other recent miRNA profiling efforts have found differentially expressed miRNA*s, such as miR-9*³⁹, miR-199*^{40,41}, miR-126*^{42,43}, miR-363*⁴⁴ miR-18*⁴⁵, miR-29c*⁴⁶ and miR-155*⁴⁷, in the pathogenesis of Waldenstroem macroglobulinemia, lung cancer and a metastasis model as well as developmental processes such as organ adhesion, respectively. In our libraries, hsa-miR-199 showed features of an α -duplex, whereas hsa-miR-9 and hsa-miR-363 displayed a more balanced expression (**Table S2**). These results are in contrast to published data suggesting that miR-199* is expressed at detectable levels in fibroblasts⁴¹, which might be attributable to differences in the profiling methodologies and cell types studied.

Thus far, the mechanisms by which strand selection occurs have not been completely resolved. Recent studies have indicated that the relative thermodynamic stability of the two ends of the duplex determines strand selection^{3,4}. In general, the strand with relatively unstable base pairs at the 5' end evades degradation. However, this concept has been challenged by studies describing tissue-dependent paired expression of miRNAs¹⁵⁻¹⁷. This could be due to tissue-dependent stability of miRNAs and miRNA*s as well as unknown extrinsic factors as suggested by the developmentally controlled arm switch observed for miR-2015 in the embryonic and adult stages of sponges⁴⁸. We could not verify such a phenomenon in our comparison of undifferentiated and differentiated ES cells. Another possibility involves the presence of a miRNA or miRNA* target in a cell, leading to a target dependent

strand selection or cell-specific modification of RISC cofactors such as TRBP, which might influence selection of the active miRNA arm. Recently, Chatterjee et al. demonstrated that mRNAs can stabilize their cognate miRNAs, suggesting coordinated RISC assembly depending on a miRNA and its target levels⁴⁹. Considering that miR-223 and miR-223* have *Igf1r* as common target, varying *Igf1r* mRNA levels in myeloid cells could theoretically contribute to the described inconsistent miR-223/miR-223* ratios. However, only few miRNA duplexes exhibited inconstant expression patterns, demonstrating that in general, miRNA strand selection is a highly preserved mechanism.

Analysis of the dynamics of miRNA strand accumulation, and the specific expression of miR-223* (**Figure S2D**) in mature myeloid cells suggested that miR-223* is relevant in myeloid differentiation. Current approaches to overexpress a miRNA utilize miRNA mimics to produce a short-term effect in cell lines. In general, bone marrow cells are very difficult to transfect and changes are usually detected after a delay of several days. We therefore took advantage of a retroviral approach by creating retroviral vectors containing mutations in either the miR-223 or the miR-223* seed region. A vector in which the miR-223* seed region was expressed but miR-223 was mutated (inactive) was sufficient to partially reverse (rescue) the enhanced CFC plating efficiency of miR223KO bm cells and thus implicating a functional role for miR-223*.

The relatively high abundance of miR-223* evident from our sequencing libraries, strongly argues that miR-223* is able to enter the RISC and therefore is functionally active. This possibility is corroborated by the frequent

enrichment of even less abundant miRNA* strands in RISC ¹⁵ and our miR-223* target screen. Here, we demonstrated that *Pik3cd*, *Cux1*, *Dlc1* and *Igf1r* are targeted by miR-223* leading to their mRNA degradation. This is especially interesting considering that a tightly regulated IGF1R/PIK3 axis, affecting amongst others PTEN and SHIP, is necessary for normal bone marrow development ^{50,51} and myeloid malignancies ³⁸. Therefore, deregulated miR-223* and miR-223 expression might associate with clinical parameters in AML patients. Indeed, high miR-223* expression levels correlate with a better overall survival in CN-AML patients, strongly highlighting a role of miR-223* in AML. We hypothesize that increased miR-223 and miR-223* levels might activate different programs, miR-223 affecting myeloid differentiation ²⁹ and miR-223* complementing miR-223 function by possibly activating apoptosis and/or inhibiting self-renewal and/or proliferation of progenitor cells (**Figure 3**) and also considered the possibility of novel SNPs in miR-223/miR-223*, as shown for miR-146. However, we could not detect any miR-223* polymorphisms in 95 profiled AML patients, which might be due to a non-significant number of profiled patients.

Our data revealed that miRNA arm accumulation underlies conserved patterns, but not exclusively the dominance of one miRNA duplex strand. Depending on the tissue, miRNA*s can be more abundant than previously assumed, implying a functional role for highly expressed miRNA*s. An important functional role for miRNA*s as illustrated by the results obtained for miR-223* in normal and malignant myeloid cells point towards a broader and thus more complicated interaction of miRNAs and disease related pathways, than previously assumed.

Authorship

Contribution: F.K., S.M.M., M.H., J.R., A.R., T.B., D.T.S., K.E., D.L. performed experiments; F.K., L.B., R.D.M., K.D., D.S., A.M., A.K., A.W., L.P. analyzed results and made the figures; F.K., R.K.H., C.B., M.M., C.J.E., H.D., F.C., S.A.A., Y.W. designed the research and wrote the paper.

Conflict-of-interest disclosure: The authors declare no competing financial interests.

Correspondence: R. Keith Humphries, Terry Fox Laboratory, BC Cancer Agency, Vancouver, BC, Canada, V5Z 1L3; email: khumphri@bccrc.ca

Acknowledgements

Supported by grants from the Terry Fox Foundation; Genome Canada/BC; the Canadian Institutes of Health; the Cancer Research Society; and the Canadian NCE Stem Cell Network. We thank Patty Rosten, Anisa Salmi and Lisa Yue for her invaluable advice and assistance. We thank all members of the Humphries' laboratory for stimulating discussions.

Contribution: F.K., S.M.M., M.H., J.R., A.R., T.B., D.T.S., K.E., D.L. performed experiments; F.K., L.B., R.D.M., K.D., D.S., A.M., A.K., A.W., L.P. analyzed results and made the figures; F.K., R.K.H., C.B., M.M., C.J.E., H.D., F.C., S.A.A., Y.W. designed the research and wrote the paper.

References

1. Bartel DP. MicroRNAs: genomics, biogenesis, mechanism, and function. *Cell*. 2004;116(2):281-297.
2. Kim VN. MicroRNA biogenesis: coordinated cropping and dicing. *Nat Rev Mol Cell Biol*. 2005;6(5):376-385.
3. Khvorova A, Reynolds A, Jayasena SD. Functional siRNAs and miRNAs exhibit strand bias. *Cell*. 2003;115(2):209-216.
4. Schwarz DS, Hutvagner G, Du T, Xu Z, Aronin N, Zamore PD. Asymmetry in the assembly of the RNAi enzyme complex. *Cell*. 2003;115(2):199-208.
5. Mah SM, Buske C, Humphries RK, Kuchenbauer F. miRNA*: a passenger stranded in RNA-induced silencing complex? *Crit Rev Eukaryot Gene Expr*. 2010;20(2):141-148.
6. Lee RC, Ambros V. An extensive class of small RNAs in *Caenorhabditis elegans*. *Science*. 2001;294(5543):862-864.
7. Lau NC, Lim LP, Weinstein EG, Bartel DP. An abundant class of tiny RNAs with probable regulatory roles in *Caenorhabditis elegans*. *Science*. 2001;294(5543):858-862.
8. Lagos-Quintana M, Rauhut R, Meyer J, Borkhardt A, Tuschl T. New microRNAs from mouse and human. *Rna*. 2003;9(2):175-179.
9. Lagos-Quintana M, Rauhut R, Yalcin A, Meyer J, Lendeckel W, Tuschl T. Identification of tissue-specific microRNAs from mouse. *Curr Biol*. 2002;12(9):735-739.
10. Morin RD, O'Connor MD, Griffith M, et al. Application of massively parallel sequencing to microRNA profiling and discovery in human embryonic stem cells. *Genome Res*. 2008;18(4):610-621.
11. Kuchenbauer F, Morin RD, Argiropoulos B, et al. In-depth characterization of the microRNA transcriptome in a leukemia progression model. *Genome Res*. 2008;18(11):1787-1797.
12. Petriv OI, Kuchenbauer F, Delaney AD, et al. Comprehensive microRNA expression profiling of the hematopoietic hierarchy. *Proc Natl Acad Sci U S A*. 2010;107(35):15443-15448.

13. Ruby JG, Jan C, Player C, et al. Large-scale sequencing reveals 21U-RNAs and additional microRNAs and endogenous siRNAs in *C. elegans*. *Cell*. 2006;127(6):1193-1207.
14. Jagadeeswaran G, Zheng Y, Sumathipala N, et al. Deep sequencing of small RNA libraries reveals dynamic regulation of conserved and novel microRNAs and microRNA-stars during silkworm development. *BMC Genomics*. 2010;11:52.
15. Okamura K, Phillips MD, Tyler DM, Duan H, Chou YT, Lai EC. The regulatory activity of microRNA* species has substantial influence on microRNA and 3' UTR evolution. *Nat Struct Mol Biol*. 2008;15(4):354-363.
16. Yang JS, Phillips MD, Betel D, et al. Widespread regulatory activity of vertebrate microRNA* species. *RNA*. 2011;17(2):312-326.
17. Ro S, Park C, Young D, Sanders KM, Yan W. Tissue-dependent paired expression of miRNAs. *Nucleic Acids Res*. 2007;35(17):5944-5953.
18. Jazdzewski K, Murray EL, Franssila K, Jarzab B, Schoenberg DR, de la Chapelle A. Common SNP in pre-miR-146a decreases mature miR expression and predisposes to papillary thyroid carcinoma. *Proc Natl Acad Sci U S A*. 2008;105(20):7269-7274.
19. Jazdzewski K, Liyanarachchi S, Swierniak M, et al. Polymorphic mature microRNAs from passenger strand of pre-miR-146a contribute to thyroid cancer. *Proc Natl Acad Sci U S A*. 2009;106(5):1502-1505.
20. Pineault N, Buske C, Feuring-Buske M, et al. Induction of acute myeloid leukemia in mice by the human leukemia-specific fusion gene NUP98-HOXD13 in concert with Meis1. *Blood*. 2003;101(11):4529-4538.
21. Johnnidis JB, Harris MH, Wheeler RT, et al. Regulation of progenitor cell proliferation and granulocyte function by microRNA-223. *Nature*. 2008;451(7182):1125-1129.
22. Pineault N, Abramovich C, Humphries RK. Transplantable cell lines generated with NUP98-Hox fusion genes undergo leukemic progression by Meis1 independent of its binding to DNA. *Leukemia*. 2005;19(4):636-643.
23. Isken F, Steffen B, Merk S, et al. Identification of acute myeloid leukaemia associated microRNA expression patterns. *Br J Haematol*. 2008;140(2):153-161.

24. Argiropoulos B, Palmqvist L, Yung E, et al. Linkage of Meis1 leukemogenic activity to multiple downstream effectors including Trib2 and Ccl3. *Exp Hematol*. 2008;36(7):845-49.
25. Heuser M, Beutel G, Krauter J, et al. High meningeoma 1 (MN1) expression as a predictor for poor outcome in acute myeloid leukemia with normal cytogenetics. *Blood*. 2006;108(12):3898-3905.
26. Cheson BD, Bennett JM, Kopecky KJ, et al. Revised recommendations of the International Working Group for Diagnosis, Standardization of Response Criteria, Treatment Outcomes, and Reporting Standards for Therapeutic Trials in Acute Myeloid Leukemia. *J Clin Oncol*. 2003;21(24):4642-4649.
27. Starczynowski DT, Kuchenbauer F, Argiropoulos B, et al. Identification of miR-145 and miR-146a as mediators of the 5q- syndrome phenotype. *Nat Med*. 2010;16(1):49-58.
28. Chen CZ, Li L, Lodish HF, Bartel DP. MicroRNAs modulate hematopoietic lineage differentiation. *Science*. 2004;303(5654):83-86.
29. Fazi F, Rosa A, Fatica A, et al. A minicircuitry comprised of microRNA-223 and transcription factors NFI-A and C/EBPalpha regulates human granulopoiesis. *Cell*. 2005;123(5):819-831.
30. Fazi F, Racanicchi S, Zardo G, et al. Epigenetic Silencing of the Myelopoiesis Regulator microRNA-223 by the AML1/ETO Oncoprotein. *Cancer Cell*. 2007;12(5):457-466.
31. Shi P, Chandra J, Sun X, et al. Inhibition of IGF-IR tyrosine kinase induces apoptosis and cell cycle arrest in imatinib-resistant chronic myeloid leukaemia cells. *J Cell Mol Med*. 2010;14(6B):1777-1792.
32. He Y, Zhang J, Zheng J, et al. The insulin-like growth factor-1 receptor kinase inhibitor, NVP-ADW742, suppresses survival and resistance to chemotherapy in acute myeloid leukemia cells. *Oncol Res*. 2010;19(1):35-43.
33. Chapuis N, Tamburini J, Cornillet-Lefebvre P, et al. Autocrine IGF-1/IGF-1R signaling is responsible for constitutive PI3K/Akt activation in acute myeloid leukemia: therapeutic value of neutralizing anti-IGF-1R antibody. *Haematologica*. 2010;95(3):415-423.

34. Chapuis N, Lacombe C, Tamburini J, Bouscary D, Mayeux P. Insulin receptor A and IGF-1R in AML - Letter. *Cancer Res.* 2010;70(17):7010; author reply 7010.
35. Guo H, Ingolia NT, Weissman JS, Bartel DP. Mammalian microRNAs predominantly act to decrease target mRNA levels. *Nature.* 2010;466(7308):835-840.
36. Li R, Pourpak A, Morris SW. Inhibition of the Insulin-like Growth Factor-1 Receptor (IGF1R) Tyrosine Kinase as a Novel Cancer Therapy Approach. *J Med Chem.* 2009. Prepublished on 2009/07/21 as DOI 10.1021/jm9002395.
37. Regha K, Latos PA, Spahn L. The imprinted mouse *Igf2r/Air* cluster--a model maternal imprinting system. *Cytogenet Genome Res.* 2006;113(1-4):165-177.
38. Wahner Hendrickson AE, Haluska P, Schneider PA, et al. Expression of insulin receptor isoform A and insulin-like growth factor-1 receptor in human acute myelogenous leukemia: effect of the dual-receptor inhibitor BMS-536924 in vitro. *Cancer Res.* 2009;69(19):7635-7643.
39. Packer AN, Xing Y, Harper SQ, Jones L, Davidson BL. The bifunctional microRNA miR-9/miR-9* regulates REST and CoREST and is downregulated in Huntington's disease. *J Neurosci.* 2008;28(53):14341-14346.
40. Lee DY, Shatseva T, Jeyapalan Z, Du WW, Deng Z, Yang BB. A 3'-untranslated region (3'UTR) induces organ adhesion by regulating miR-199a* functions. *PLoS ONE.* 2009;4(2):e4527.
41. Kim S, Lee UJ, Kim MN, et al. MicroRNA miR-199a* regulates the MET proto-oncogene and the downstream extracellular signal-regulated kinase 2 (ERK2). *J Biol Chem.* 2008;283(26):18158-18166.
42. Kalscheuer S, Zhang X, Zeng Y, Upadhyaya P. Differential expression of microRNAs in early-stage neoplastic transformation in the lungs of F344 rats chronically treated with the tobacco carcinogen 4-(methylnitrosamino)-1-(3-pyridyl)-1-butanone. *Carcinogenesis.* 2008;29(12):2394-2399.
43. Musiyenko A, Bitko V, Barik S. Ectopic expression of miR-126*, an intronic product of the vascular endothelial EGF-like 7 gene, regulates protein translation and invasiveness of prostate cancer LNCaP cells. *J Mol Med.* 2008;86(3):313-322.

44. Roccaro AM, Sacco A, Chen C, et al. microRNA expression in the biology, prognosis, and therapy of Waldenstrom macroglobulinemia. *Blood*. 2009;113(18):4391-4402.
45. Tsang WP, Kwok TT. The miR-18a* microRNA functions as a potential tumor suppressor by targeting on K-Ras. *Carcinogenesis*. 2009;30(6):953-959.
46. Pass HI, Goparaju C, Ivanov S, et al. hsa-miR-29c* is linked to the prognosis of malignant pleural mesothelioma. *Cancer Res*. 2010;70(5):1916-1924.
47. Zhou H, Huang X, Cui H, et al. miR-155 and its star-form partner miR-155* cooperatively regulate type I interferon production by human plasmacytoid dendritic cells. *Blood*. 2010;116(26):5885-5894.
48. Grimson A, Srivastava M, Fahey B, et al. Early origins and evolution of microRNAs and Piwi-interacting RNAs in animals. *Nature*. 2008;455(7217):1193-1197.
49. Chatterjee S, Grosshans H. Active turnover modulates mature microRNA activity in *Caenorhabditis elegans*. *Nature*. 2009;461(7263):546-549.
50. Helgason CD, Damen JE, Rosten P, et al. Targeted disruption of SHIP leads to hemopoietic perturbations, lung pathology, and a shortened life span. *Genes Dev*. 1998;12(11):1610-1620.
51. Shimon I, Shpilberg O. The insulin-like growth factor system in regulation of normal and malignant hematopoiesis. *Leuk Res*. 1995;19(4):233-240.

Table 1. Top 5 of the highest expressed in mirBase annotated miRNA*s from each library.

	mouse leukemia 1	mouse leukemia 2	ES undiff	ES diff	Leukemia 1
miRNA/miRNA* reads^	819023/25750	666362/29718	1062508/130652	1275288/51895	872298/10202
%miRNA*	3.1	4.5	12.3	4.1	1.2
Top5 miRNA**	mmu-miR-140*	mmu-miR-140*	hsa-miR-302a*	hsa-miR-302a*	hsa-miR-30e*
	mmu-miR-30e*	mmu-miR-30e*	hsa-miR-30e*	hsa-miR-30e*	hsa-miR-493*
	mmu-miR-322*	mmu-miR-322*	hsa-miR-25*	hsa-miR-30a*	hsa-miR-181a*
	mmu-miR-106b*	mmu-miR-106b*	hsa-miR-92b*	hsa-miR-25*	hsa-miR-221*
	mmu-miR-27b*	mmu-miR-17*	hsa-miR-221*	hsa-miR-92b*	hsa-miR-25*

	Leukemia 2	Leukemia 3	Prostate 2	Prostate 1	Colon
miRNA/miRNA* reads^	1730532/30466	1328614/6483	1251565/5273	2357704/7679	4661901/42458
%miRNA*	1.8	0.5	0.4	0.3	0.9
Top5 miRNA**	hsa-miR-30e*	hsa-miR-25*	hsa-miR-30a*	hsa-miR-221*	hsa-miR-221*
	hsa-miR-223*	hsa-miR-374a*	hsa-miR-25*	hsa-miR-25*	hsa-miR-30e*
	hsa-miR-92a-1*	hsa-miR-30e*	hsa-miR-223*	hsa-miR-21*	hsa-miR-106b*
	hsa-miR-17*	hsa-miR-221*	hsa-miR-30e*	hsa-miR-30e*	hsa-miR-374a*
	hsa-miR-25*	hsa-miR-223*	hsa-miR-221*	hsa-miR-155*	hsa-miR-21*

^only annotated miRNA*s

Table 2. Distribution (%) of the various miRNA/miRNA* ratio groups in each library.

% of all ratios	mouse leukemia 1	mouse leukemia 2	ES undiff	ES diff	Leukemia 1	average for all libraries
>100	47.9	50.9	42.0	43.4	40.7	50.4
100-10	24.4	25.4	30.9	27.4	25.2	23.7
<10	12.6	12.3	14.0	15.1	15.0	12.9
<1	15.1	11.4	13.1	13.9	19.1	12.9
% of all ratios	Leukemia 2	Leukemia 3	Prostate 1	Prostate 2	Colon	Breast
>100	47.0	60.6	61.2	56.4	54.2	50.5
100-10	28.5	22.2	18.1	20.8	19.6	18.2
<10	14.6	10.1	8.6	10.7	11.7	17.7
<1	9.9	7.1	12.1	12.1	14.5	13.6

Table 3. Examples of α - and β -duplexes.

Ratio (miRNA/miRNA*)	let-7a	miR-103	miR-320a	miR-107	miR-101
Mouse leukemia 1	15773.5	40465	9354	21195	1881
Mouse leukemia 2	31822.66667	26642	5505	16623	1237
ES undiff	11179	207069	25214	20119	8012
ES diff	4986	269177	2228	19099	3880
Leukemia 1	6349	46489	37114	32102	19329
Leukemia 2	5364.58	68834	8378.5	17958	6974
Leukemia 3	2701.321839	31017	3095	11571	5629
Prostate 1	47738	35289	2782	7347	2555
Prostate 2	14021.92308	31233	2090	9151	1676
Colon	16389.34043	309168	109730	6041	25246
	a-duplex	a-duplex	a-duplex	a-duplex	a-duplex

Ratio (miRNA/miRNA*)	miR-30e	miR-17	miR-30a	miR-32	miR-625
Mouse leukemia 1	0.754216867	1.703703704	n/e	n/e	n/e
Mouse leukemia 2	0.828804348	1.508274232	n/e	n/e	n/e
ES undiff	0.141397289	4.563953488	2.751046025	0.888888889	0.581699346
ES diff	0.365884431	2.691432904	3.246661102	1.636363636	0.520958084
Leukemia 1	0.013737836	0.655882353	0.5	3	1.474358974
Leukemia 2	1.716995682	1.081261596	2.735955056	5.538461538	0.785714286
Leukemia 3	0.849372385	1.05952381	0.230769231	3.75	0.388888889
Prostate 1	0.235474006	3.344827586	2.492537313	2.166666667	1.4
Prostate 2	0.153729072	7.416149068	1.145530146	1.8	6.428571429
Colon	0.974157734	8.263414634	3.492307692	1.6	1.125
	b-duplex	b-duplex	b-duplex	b-duplex	b-duplex

n/e = not expressed

Table 4. MiRNA duplexes with dynamic arm expression.

Ratio (miRNA/miRNA*)	miR- 106b	miR- 1307	miR-16	miR- 1975	miR- 223	miR- 23b	miR-365
Mouse leukemia 1	0.62	n/e	767.75	n/e	0.17	1.16	0.28
Mouse leukemia 2	1.00	n/e	449.00	n/e	2.02	0.68	287.00
ES undiff	1.89	4.41	17.01	10.06	n/e	2.40	4.00
ES diff	3.61	0.97	32.88	15.21	n/e	2.98	4.06
Leukemia 1	5.67	0.26	20.59	5.80	28.28	1.51	15.50
Leukemia 2	2.68	1.49	121.18	0.39	1.41	4.24	126.00
Leukemia 3	8.94	0.26	11.62	9.36	21.82	3.92	26.00
Prostate 1	12.65	0.58	464.13	0.10	1.41	14.00	0.67
Prostate 2	19.67	1.97	1262.44	0.31	0.52	34.37	0.74
Colon	0.28	21.69	0.58	0.10	n/e	0.55	0.16

Table 5. Clinical characteristics and correlation of prognostic markers in 92 profiled AML patients dichotomized to the 75% percentile.

Clinical parameter	Low miR223*	High miR223*	p-value
Cases	(n = 69)	(n = 23)	
Age, years			0.28
Median	48	48	
range	17-60	25-60	
Sex			0.55
male - no. (%)	38 (55)	11 (48)	
female - no. (%)	31 (45)	12 (52)	
FAB-Subtype			0.73
M0 - no. (%)	1 (2)	0 (0)	
M1 - no. (%)	7 (10)	2 (9)	
M2 - no. (%)	16 (23)	4 (17)	
M4 - no. (%)	30 (43)	11 (48)	
M5 - no. (%)	11 (16)	3 (13)	
M6 - no. (%)	1 (2)	2 (9)	
M7 - no. (%)	0	0 (0)	
missing data - no. (%)	3 (4)	1 (4)	
Percentage blasts in sample			0.25
median (%)	80	75	
missing data – no. (%)	5	0	
Type of AML			0.85
de novo - no. (%)	61 (88)	20 (87)	
post MDS/secondary - no. (%)	8 (12)	3 (13)	
WBC count			0.78
median - (x10⁹/l)	27	29	
range - (x10⁹/l)	1 – 328	1-170	
ECOG performance status			0.14
0 or 1 - no. (%)	66 (96)	20 (87)	
2 - no. (%)	3 (4)	3 (13)	
FLT3-ITD			0.42
mutated – no. (%)	21 (30)	5 (22)	
NPM1			0.33
mutated – no. (%)	36 (52)	15 (65)	
missing – no. (%)	5 (7)	1 (4)	
NPM1mutated/FLT3-ITD negative			0.25
(low risk) – no. (%)	23 (33)	11 (48)	
missing – no. (%)	5 (7)	1 (4)	
CEBPA			0.51
mutated – no. (%)	10 (14)	5 (22)	
missing – no. (%)	5 (7)	0 (0)	

Figure Legends

Figure 1. Deep sequencing profile of 10 miRNA libraries. **A** Examples of miRNA/miRNA* duplexes with high, intermediate and low ratios across all tissues. The x-axis indicates all sequencing libraries and the y-axis all calculated miRNA:miRNA* ratios. **B** Examples of miRNA duplexes with dynamic arm expression. The x-axis indicates all sequencing libraries and the y-axis all calculated miRNA:miRNA* ratios. **C** Experimental setup to test the activity of miR-223 and miR-223* in CFC assays. **D** Colony counts for each experimental arm (n=3).

Figure 2. Quantification of miR-223* and miR-223* targets. **A** Venn diagram comparing differentially expressed genes (shown as transcript cluster IDs), assessed by mRNA microarrays with predicted mRNA targets (shown as transcript cluster IDs). **B** Quantification of Cux1, Igf1r, Dlc1 and Pik3cd by real-time PCR in miR-223KO cells, expressing strand inactivating constructs (n=3). **C** IGF1R Luciferase assay. **D** Comparison of miR-223 and miR-223* levels in healthy donors (n=10) and CN-AML patients (n=92). The Y-Axis depicts Δ CT (miRNA-miR-92) values. **E** miR-223* levels measured in 92 CN-AML patients by real-time PCR. Overall survival was plotted on miR-223* levels dichotomized to the 75th percentile. *p<0.05

Figure 3. Proposed model of a miR-223* and miR-223 crosstalk.

Figure 1

From bloodjournal.hematologylibrary.org at The University of British Columbia Library on July 12, 2011. For personal use only.

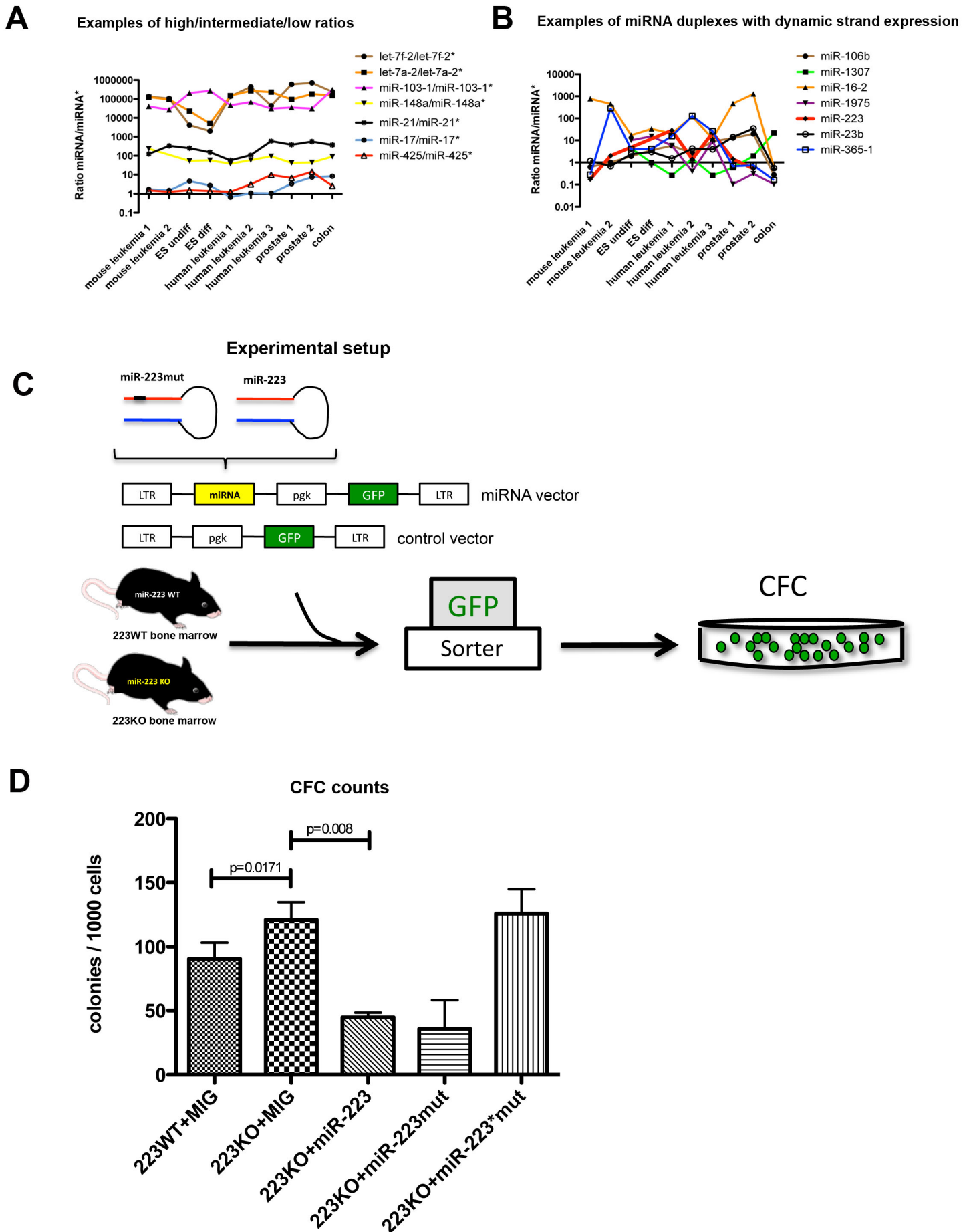


Figure 2

From bloodjournal.hematologylibrary.org at The University of British Columbia Library on July 12, 2011. For personal use only.

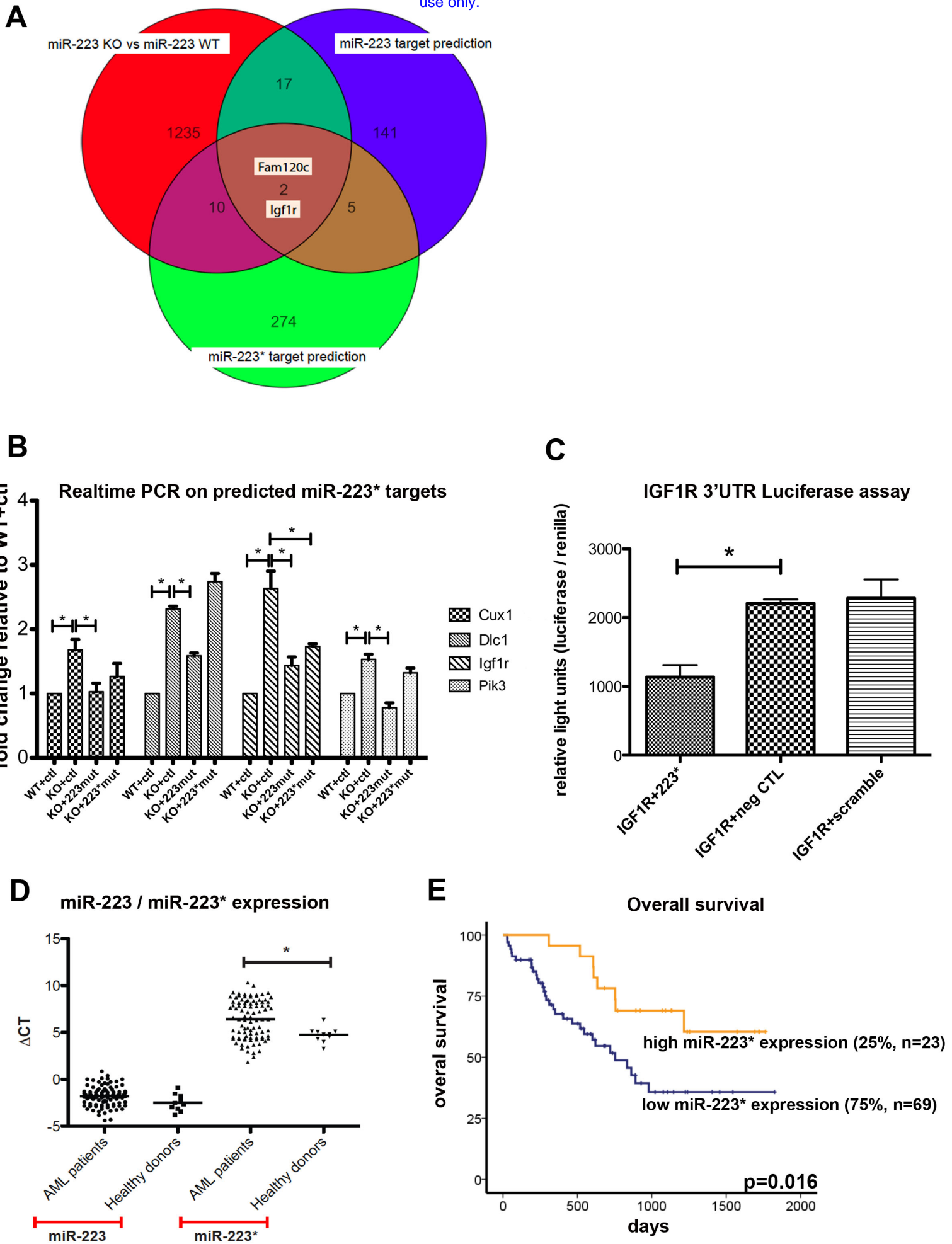


Figure 3

